Suppression of arabidopsis GGLT1 affects growth by reducing the L-galactose content and borate cross-linking of rhamnogalacturonan-II

Julien Sechet, Soe Htwe, Breeanna Urbanowicz, Abigail Agyeman, Wei Feng, Toshiki Ishikawa, Marianne Colomes, Kavitha Satish Kumar, Maki Kawai-Yamada, Jose R. Dinneny, et al.

the plant journal

SEB Society for Experimental Biology

The Plant Journal (2018) **96,** 1036–1050 doi: 10.1111/tpj.14088

Suppression of Arabidopsis GGLT1 affects growth by reducing the L-galactose content and borate cross-linking of rhamnogalacturonan-II

Julien Sechet[1,2,†], Soe Htwe[1,2], Breeanna Urbanowicz[3], Abigail Agyeman[3,‡], Wei Feng[4], Toshiki Ishikawa[5], Marianne Colomes[1,2,§], Kavitha Satish Kumar[1,2], Maki Kawai-Yamada[5], José R. Dinneny[4,6], Malcolm A. O'Neill[3] and Jenny C. Mortimer[1,2,*]

[1]*Joint BioEnergy Institute, Emeryville, CA 94608, USA,*
[2]*Biosciences Area, Lawrence Berkeley National Laboratory, Berkeley, CA 94720, USA,*
[3]*Complex Carbohydrate Research Center, The University of Georgia, Athens, GA 30602, USA,*
[4]*Department of Plant Biology, Carnegie Institute for Science, Stanford, CA 94305, USA,*
[5]*Graduate School of Science and Engineering, Saitama University, Saitama 338-8570, Japan, and*
[6]*Department of Biology, Stanford University, Stanford, CA 94305, USA*

Received 16 May 2018; revised 14 August 2018; accepted 20 August 2018; published online 11 September 2018.
*For correspondence (e-mail: jcmortimer@lbl.gov).
[†]Present address: INRA, Versailles 78000, France.
[‡]Present address: School of Pharmacy, South University, Savannah,GA 31406, USA.
[§]Present address: Nutribio, Paris 75440, France.

SUMMARY

Boron is a micronutrient that is required for the normal growth and development of vascular plants, but its precise functions remain a subject of debate. One established role for boron is in the cell wall where it forms a diester cross-link between two monomers of the low-abundance pectic polysaccharide rhamnogalacturonan-II (RG-II). The inability of RG-II to properly assemble into a dimer results in the formation of cell walls with abnormal biochemical and biomechanical properties and has a severe impact on plant productivity. Here we describe the effects on RG-II structure and cross-linking and on the growth of plants in which the expression of a GDP-sugar transporter (GONST3/GGLT1) has been reduced. In the *GGLT1*-silenced plants the amount of L-galactose in side-chain A of RG-II is reduced by up to 50%. This leads to a reduction in the extent of RG-II cross-linking in the cell walls as well as a reduction in the stability of the dimer in the presence of calcium chelators. The silenced plants have a dwarf phenotype, which is rescued by growth in the presence of increased amounts of boric acid. Similar to the *mur1* mutant, which also disrupts RG-II cross-linking, *GGLT1*-silenced plants display a loss of cell wall integrity under salt stress. We conclude that GGLT1 is probably the primary Golgi GDP-L-galactose transporter, and provides GDP-L-galactose for RG-II biosynthesis. We propose that the L-galactose residue is critical for RG-II dimerization and for the stability of the borate cross-link.

Keywords: boron, golgi, nucleotide-sugar transporter, pectin, rhamnogalacturonan II.

INTRODUCTION

In flowering plants, a primary role for boron is to form a diester cross-link between two monomers of rhamnogalacturonan-II (RG-II), a pectic polysaccharide present in the cell walls of all vascular plants (O'Neill *et al.*, 2004). Rhamnogalacturonan-II is a structurally complex domain of pectin (Figure 1; Atmodjo *et al.*, 2013), which comprises 12 different monosaccharides that are linked together by at least 20 different glycosidic linkages (O'Neill *et al.*, 2004). Nevertheless, its structure is largely conserved in vascular plants (Matsunaga *et al.*, 2004; Pabst *et al.*, 2013). The majority of RG-II exists in the wall as a dimer that is generated by forming a borate diester between the D-apiose of side chain A of two RG-II molecules. The inability of RG-II to properly assemble into a dimer results in the formation of cell walls with abnormal biochemical and biomechanical properties and has a severe impact on plant productivity.

Nevertheless, the mechanisms that drive the interactions between borate and RG-II are poorly understood (Chormova *et al.*, 2014; Funakawa and Miwa, 2015).

There is increasing evidence that alteration of RG-II structure and cross-linking have severe impacts on plant growth, development and viability. To date, the only characterized RG-II biosynthetic enzymes are the rhamnogalacturonan xylosyl transferases (RGXT1–4, CAZy family GT77) (Lombard *et al.*, 2014), which catalyze the transfer of xylose from UDP-xylose to fucose to form α-xylose-(1,3)-fucose *in vitro* (Egelund *et al.*, 2008; Petersen *et al.*, 2009). Inactivation of *RGXT1* and *-2* has no discernible effect on plant growth or RG-II structure (Egelund *et al.*, 2006), implying redundancy of function, whereas mutations affecting *RGXT4* lead to defects of root and pollen tube growth that are lethal (Fangel *et al.*, 2011; Liu *et al.*, 2011). Mutations that prevent the synthesis of UDP-Api and CMP-Kdo are also lethal and provide further evidence for the essential role of RG-II in plant growth (Delmas *et al.*, 2003, 2008; Mølhøj *et al.*, 2003; Ahn *et al.*, 2006). In the dwarf Arabidopsis mutant *murus* 1 (*mur1*) L-galactose replaces L-fucose in several cell wall polysaccharides, including RG-II, because the plant is unable to produce GDP-fucose in its shoots as it lacks GDP-D-mannose-4,6-dehydratase GMD1 (Bonin *et al.*, 1997). This has been shown to result in the incomplete formation of the A side-chain of RG-II, which in turn reduces the stability of the borate cross-linked dimer (Bonin *et al.*, 1997; O'Neill *et al.*, 2001). Thus, the structural integrity of RG-II is probably important for its biological functions.

Pectic and hemicellulosic polysaccharides are synthesized in the Golgi apparatus using activated donor substrates, typically in the form of nucleotide diphosphate-linked (NDP-) sugars (Davis *et al.*, 2010). However, most NDP-sugars are synthesized in the cytosol (Bar-Peled and O'Neill, 2011). Thus, NDP-sugar transporters (NSTs) are required to provide substrates for glycan synthesis (Rautengarten *et al.*, 2016). The Golgi-localized NST (GONST) sub-family, which forms part of clade IIIa of the NST/triose phosphate transporter superfamily (Rautengarten *et al.*, 2014), comprises four members related to GONST1 (At2g13650), the first nucleotide sugar transporter described in Arabidopsis (Baldwin *et al.*, 2001; Handford *et al.*, 2004). The members of this family are the only Arabidopsis NSTs that contain a predicted GDP-binding motif (Handford *et al.*, 2004). Arabidopsis is known to synthesize four GDP-linked sugars: GDP-L-fucose, GDP-L-galactose, GDP-D-glucose and GDP-D-mannose. GDP-mannose for the glycosylation of glycosylinositolphosphorylceramides (GIPCs) is transported into the Golgi by GONST1 (Mortimer

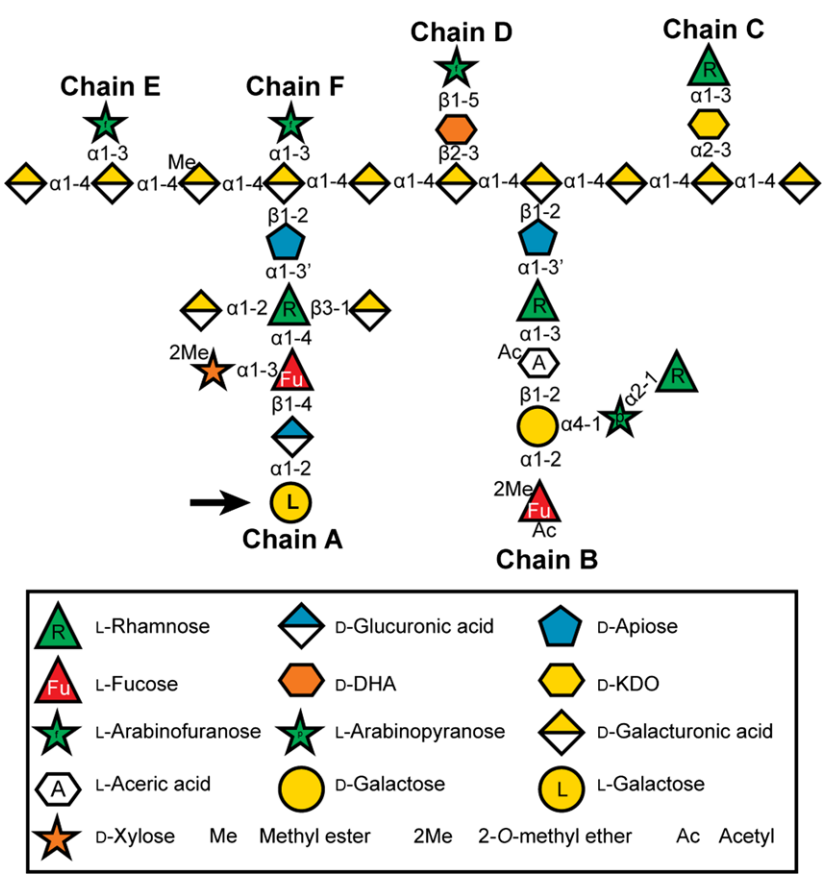

Figure 1. The glycosyl sequence of Arabidopsis rhamnogalacturonan-II (RG-II) (modified from Ndeh *et al.*, 2017). Sugars are represented using the Symbol Nomenclature for Glycans (SNFG; Varki *et al.*, 2015), with minor modifications to enable color-blind readers to distinguish L-fucose and L-rhamnose, and with a white hexagon to represent aceric acid since it does not currently have a SNFG designation (D-KDO, 3-deoxy-D-manno-octulosonic acid; D-DHA, 2-keto-3-deoxy-D-lyxo-heptulosaric acid). The L-galactose residue, which is reduced in the hairpin *GGLT1* lines described in this publication, is marked with an arrow.

et al., 2013; Fang *et al.*, 2016), whereas GDP-fucose is transported by GONST4, which has been renamed GDP-fucose transporter1 (GFT1) (Rautengarten *et al.*, 2016). No Golgi-localized GDP-L-galactose transporters have been identified to date. GDP-L-galactose is synthesized from GDP-mannose in the cytosol by GDP-mannose epimerase (GME) (Gilbert *et al.*, 2009; Mounet-Gilbert *et al.*, 2016). Most GDP-L-galactose is then converted, via L-galactose, into L-ascorbate (vitamin C), which is important for maintaining redox balance in the cell, particularly under abiotic or biotic stress (Smirnoff, 2000). However, some GDP-L-galactose is required for cell wall polysaccharide synthesis since L-galactose is present in side chain A of RG-II, in the side-chains of xyloglucan from a limited number of plant species (although not Arabidopsis) (Hantus *et al.*, 1997) and in corn bran glucuronoarabinoxylan (Rogowski *et al.*, 2015).

Here we provide evidence that *GONST3* (At1g76340) probably encodes a Golgi-localized GDP-L-galactose transporter, which we rename *Golgi GDP-L-galactose transporter1* (*GGLT1*). We used RNA interference (RNAi) to suppress *GGLT1* expression in Arabidopsis, since complete loss of *GGLT1* is lethal. Plants with decreased *GGLT1* expression have growth defects, which are rescued by increasing the amount of borate in their growth medium. Chemical analysis of the cell walls of *GGLT1* knock-down plants revealed a substantial reduction in the L-galactose decoration of RG-II, which is correlated with a decrease in the proportion of RG-II dimer in the wall and a decrease in the stability of the crosslink. Our results underscore the importance of RG-II to plant survival, and highlight an unexpectedly critical role for L-galactose in borate cross-linking of this unusual pectic polysaccharide.

RESULTS

Subcellular localization of GGLT1

Publicly available gene expression data reveal that *GGLT1* is a ubiquitously expressed gene, with a level of expression that is slightly lower than *GONST1* and *GFT1* (Handford *et al.*, 2004; Rautengarten *et al.*, 2016). In an earlier study, the subcellular localization of GGLT1 was not determined because tagged *GGLT1* could not be expressed *in vivo* (Handford *et al.*, 2004). To overcome this issue, the full-length *GGLT1* coding sequence tagged with a fluorescent protein was introduced into onion epidermal cells by biolistic transformation. Confocal imaging revealed that the fluorescently tagged GGLT1 gave a punctate signal that co-localized with a Golgi marker (Lao *et al.*, 2014) (Figure S1 in the online Supporting Information).

GGLT1 is essential for plant growth and development

No Arabidopsis lines carrying a T-DNA insertion in the *GGLT1* open reading frame have been reported. A single T-DNA line (SAIL_71_H10), with an insertion 841 bp upstream of the start of transcription was obtained, but we were unable to identify any plants homozygous for the T-DNA insertion despite screening at least 30 different seedlings. Therefore, we took a targeted gene-knockdown approach and generated RNAi transgenic lines with a hairpin (hp) RNA construct, which specifically targeted *GGLT1*. Forty independent hp*GGLT1* transformants were screened, and four were selected for characterization (Figure 2). These lines all had rosettes which were smaller than the empty vector (EV) control (Figure 2a).

Quantitative real-time PCR (qPCR) showed that in the rosette leaves of the hpRNAi lines 1–3 (Figure 2b) the levels of *GGLT1* silencing were similar (about an 80–85% decrease relative to the EV control). These data, together with the lack of T-DNA lines, suggest that stronger suppression of *GGLT1* or null mutants will produce plants that are not viable. The expression of *GFT1*, the closest homolog of *GGLT1*, was not affected in lines 3 and 4 but was decreased by up to 50% in lines 1 and 2 (Figure 2c).

The monosaccharide compositions of the walls, including fucose, were not significantly altered in any of the hpRNAi lines (Figure 2d, Data S1), indicating that their phenotypes do not result from altered fucosylation of cell wall glycans and are thus a consequence of *GGLT1* silencing. Moreover, the shortened petiole phenotype that is characteristic of silenced *GFT1* plants as well as *mur1* plants, which also have cell walls with reduced fucose (Reiter *et al.*, 1993; Rautengarten *et al.*, 2016), was not observed in our hp*GGLT1* knock-down lines (Figure 2a).

Xyloglucan structure is not altered and GIPC glycosylation is unaffected in hp*GGLT1* plants

L-Galactose replaces L-fucose in the xyloglucan formed by *mur1* and *GFT1*-silenced plants where GDP-fucose synthesis or transport is perturbed (O'Neill *et al.*, 2001; Rautengarten *et al.*, 2016). Since GGLT1 and GFT1 are closely related NSTs, we first determined if xyloglucan fucosylation is altered in hp*GGLT1* (Lerouxel *et al.*, 2002). No differences were discernible in the matrix-assisted laser desorption–ionization time-of-flight (MALDI-TOF) mass spectra of the oligosaccharides generated by enzymatic fragmentation of the xyloglucan from hp*GGLT1* and EV control lines (Figure S2). The presence of fucosylated side chains, together with no substantial increase in the abundance of galactosylated side-chains in the hp*GGLT1* lines, supports our assertion that GDP-fucose transport is unaffected in the silenced plants.

GGLT1 is in the same NST subclade as GONST1, which provides GDP-mannose specifically for GIPC glycosylation, as opposed to polysaccharide biosynthesis (Mortimer *et al.*, 2013). Although glycosylation of GIPCs is still poorly understood, it is possible that other GDP-sugars, in

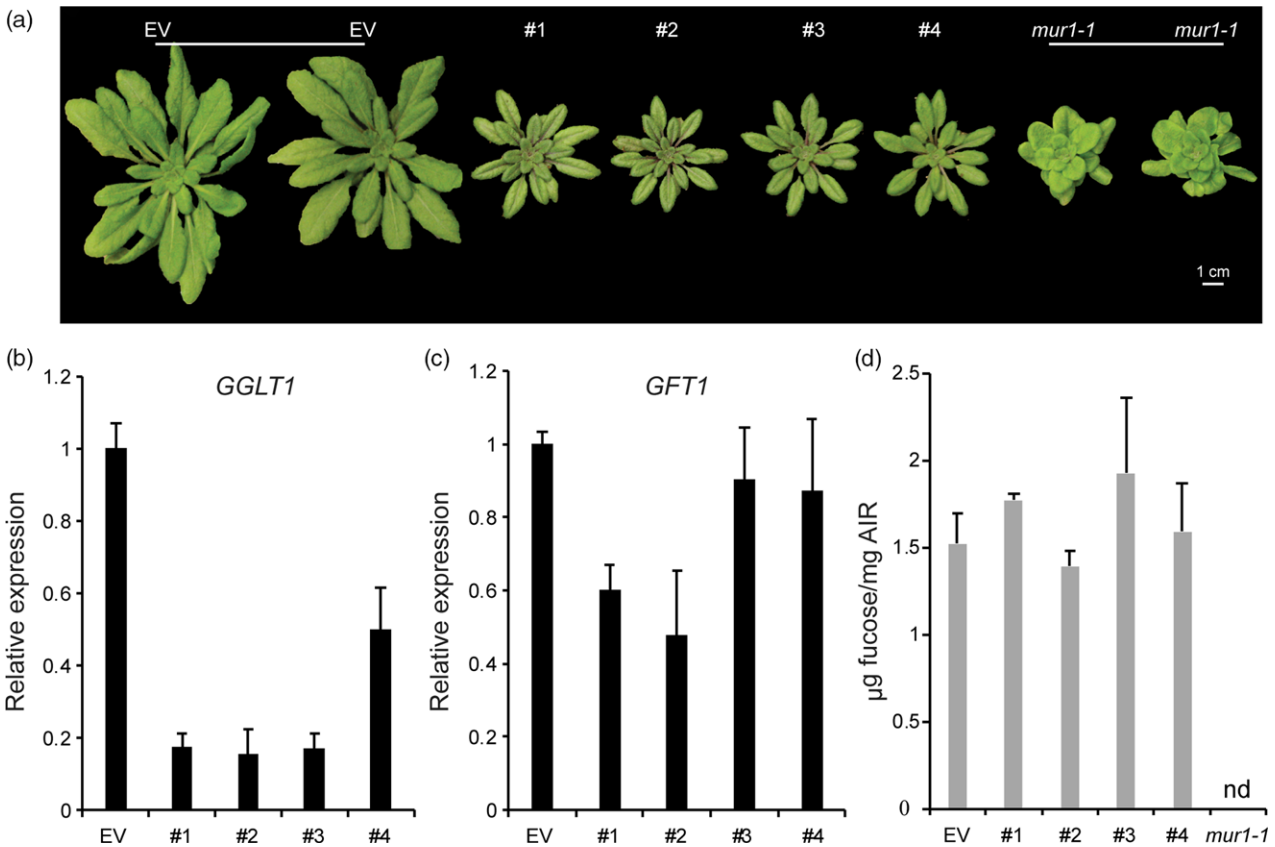

Figure 2. Characterization of hairpin (hp) *GGLT1*. (a) Empty vector control (EV) and four hp*GGLT1* lines grown on soil for 1 month. (b) Relative expression of *GGLT1* and (c) its closest homologue, *GFT1*, in the four hpRNAi lines selected determined by quantitative PCR. (d) The cell wall fucose content of the selected lines. Alcohol-insoluble residue was hydrolyzed with 2 M trifluoroacetic acid, and the released monosaccharides analyzed by high-performance anion exchange chromatography with pulsed amperometric detection. See Data S2 for complete data. Data are the mean of three biological replicates, error bars are the standard deviation. [Colour figure can be viewed at wileyonlinelibrary.com].

addition to GDP-mannose are required. Therefore, we used thin layer chromatography (TLC; Figure S3) and LC-MS (Data S2) to determine the GIPC glycan composition of hp*GGLT1*. No major differences were discernible between hp*GGLT1* and EV GIPCs. The overall sphingolipidomic composition was also unchanged (Data S2). Together, the combined results of these studies show that *GGLT1* does not encode a Golgi-localized protein involved in the transport of GDP-L-fucose or GDP-D-mannose. Thus, we next investigated if the L-galactose content of the wall was altered in the *GGLT1* suppressed lines.

Hairpin GGLT1 shows a specific decrease in RG-II L-galactose

No significant differences were detected in the wall monosaccharide compositions of leaves from soil-grown EV and hp*GGLT1* lines (Figure 2d, Data S1). This is not surprising since in primary cell walls D-galactose is far more abundant than L-galactose (Baydoun and Fry, 1988). Moreover, D-galactose and L-galactose are not separated when the monosaccharide composition of the cell wall is determined by high-performance anion exchange chromatography with pulsed amperometric detection (HPAEC-PAD).

Rhamnogalacturonan-II is the only known L-galactose-containing polysaccharide present in wild-type Arabidopsis cell walls, so we next determined whether the structure of RG-II differed in hp*GGLT1* and EV plants. Material enriched in pectic polysaccharides, including RG-II, was obtained by extracting hp*GGLT1* and EV leaf alcohol-insoluble residue (AIR) with ammonium oxalate, a calcium chelator. This material was then treated with endopolygalacturonase (EPG) and the products separated by size-exclusion chromatography (SEC) (Figure 3a). This separates RG-II from RG-I and oligogalacturonides, and also separates the RG-II monomer and dimer. In EV control plants the dimer accounts for 77% of the total RG-II isolated from the wall. Somewhat unexpectedly, the dimer accounts for only 49% of the hp*GGLT1* RG-II, and makes up only 6% of the RG-II in *mur1-1* (Figure 3a, Table S1). This led us to suspect that the ability of hp*GGLT1* RG-II to form dimers or the stability of those dimers had been altered. The latter notion is

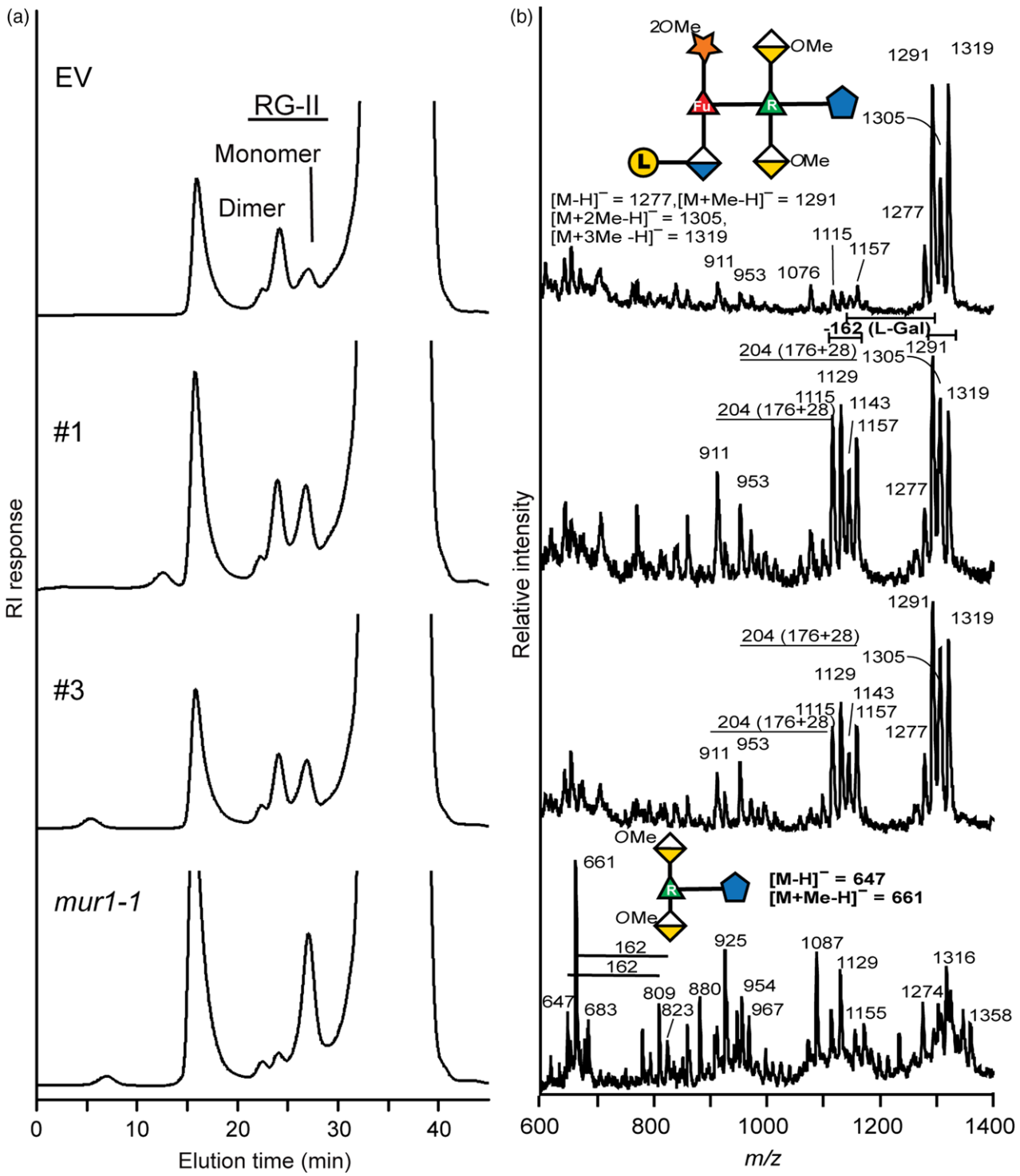

Figure 3. Borate cross-linking of rhamnogalacturonan-II (RG-II) is reduced in the hairpin (hp) *GGLT1* lines. (a) The size exclusion chromatography profiles of the material generated by endopolygalacturonase treatment of the oxalate-soluble materials from the alcohol-insoluble residues of the empty vector (EV) control, hp*GGLT1* lines and *mur1-1*. The positions of the RG-II monomer and dimer are shown. (b) The negative ion matrix-assisted laser desorption–ionization time-of-flight mass spectrum of side-chain A generated by selective acid hydrolysis of RG-II. The predominant oligosaccharide (*m*/*z* 1277, 1291, 1305 and 1319) in the empty vector corresponds to side-chain A. In the hp*GGLT1* lines between 30% and 50% of side-chain A lacks a hexose (*m*/*z* 1115, 1129, 1143 and 1157). The mass difference of 14 Da corresponds to differences in the extent of *O*-methylation of side-chain A. As previously reported (O'Neill *et al.*, 2001) *mur1-1* RG-II contains little if any intact side-chain A. The oligosaccharide structures are represented using a modified Symbol Nomenclature for Glycans nomenclature. See Figure 1 for details.

supported by our SEC data for the RG-II released by EPG treatment of the AIR (Table S2). Under these conditions, in the absence of a chelating agent, the dimer accounted for 97% of the RG-II in the EV control plants (1.2-fold more dimer than in the oxalate fraction), 87% of the RG-II in the hp*GGLT1* lines (1.8-fold more dimer than in the oxalate fraction) and 70% of the *mur1-1* (12-fold more dimer than in the oxalate fraction). These results, together with data showing that calcium chelators partially convert the RG-II dimer to the monomer (Matoh and Kobayashi, 1998; Fleischer *et al.*, 1999), strongly suggest that both the extent of formation and the stability of the borate cross-link in RG-II are affected in the hp*GGLT1* lines.

The differences in dimer abundance in the EPG and oxalate fractions were most pronounced with *mur1-1* plants. This mutant produces RG-II that lacks L-galactose because its A side-chain is truncated (Pabst *et al.*, 2013), which led us to suspect that the L-galactose content of side-chain A of the RG-II from the hp*GGLT1* lines may also be reduced.

To determine if RG-II structure is indeed altered in the hp*GGLT1* lines we isolated the total RG-II from the silenced and EV plants. Glycosyl residue composition analyses showed that D/L-galactose was reduced by about 35% in the most strongly affected hp*GGLT1* lines (Table 1). We then treated the RG-II with warm trifluoroacetic acid (TFA) (Pabst *et al.*, 2013) to release side chains A and B. The MALDI-TOF MS analysis showed that a substantial portion of side-chain A from hp*GGLT1* RG-II existed as a heptasaccharide whereas virtually all the A chain from the EV control was present as an octasaccharide (Figure 3b). The A side-chains produced by hp*GGLT1* and EV plants differ in mass by 162 Da, corresponding to a hexose residue, which we consider likely to be L-galactose. The side-chain B of RG-II contains a D-galactose residue (see Figure 1). However, no differences were discernible in the structures of this side-chain from RG-II of hp*GGLT1* and EV plants (Figure S4). Our structural data provide compelling evidence that the abundance of terminal L-galactose present on the A side-chain of RG-II is specifically affected in hp*GGLT1* plants.

Table 1 Monosaccharide composition of rhamnogalacturonan-II (RG-II) isolated from hairpin *GGLT1* plants. RG-II was isolated by size exclusion chromatography and then hydrolyzed with trifluoroacetic acid. The monosaccharides released were determined by high-performance anion exchange chromatography with pulsed amperometric detection and by gas-liquid chromatography, and are presented as mol%.

	EV	#1	#3
MeFuc	4	4	4
Fuc	4	4	5
Rha	15	16	15
Ara	14	15	13
MeXyl	4	4	4
Api	9	10	10
AceA	3	3	4
Gal	15	9	10
GalA	29	32	31
GlcA	3	3	4

EV, empty vector; MeFuc, 2-*O*-methyl fucose; Fuc, fucose; Rha, rhamnose; Ara, arabinose; MeXyl; 2-*O*-methyl xylose; Api, apiose; AceA, aceric acid; Gal, galactose; GalA, galactutonic acid; GlcA, glucuronic acid.

To confirm the identity of the missing hexose in side-chain A, the RG-II monomers generated from the hp*GGLT1* and EV plants were treated with a recently identified α-L-galactosidase (CAZY family glycosyl hydrolase (GH) 95) from *Bacteroides thetaiotaomicron* that specifically removes the terminal L-galactose from side-chain A of RG-II (Ndeh *et al.*, 2017). Galactose was the only monosaccharide detected by HPAEC-PAD following hydrolysis of EV control RG-II with the α-L-galactosidase (Figure 4a). Less galactose was released from the RG-II of the hp*GGLT1*-silenced lines relative to the control (Figure 4b,c). The MALDI-TOF MS analysis of side-chain A, released by mild TFA hydrolysis following α-L-galactosidase treatment of RG-II monomer, revealed that the predominant oligosaccharides (*m/z* 1115, 1129, 1143 and 1157) in the EV control plants correspond to side-chain A lacking L-galactose (Figure 4d; compare with the untreated EV side-chain A in Figure 3b). The L-galactose was almost completely removed as only low-intensity signals corresponding to L-galactosylated A side-chains were discernible (*m/z* 1277, 1291 and 1305) (Figure 4d). The mass spectra of side-chain A from both hp*GGLT1* silenced lines are similar to that of the EV control (Figure 4e,f), demonstrating that the mass difference of 162 Da between the EV control and hp*GGLT1* lines in Figure 3(b) is due to the specific loss of L-galactose.

It has been proposed that pectin domains may be linked covalently to each other or to other cell wall components (e.g. Popper and Fry, 2008; Atmodjo *et al.*, 2013; Tan *et al.*, 2013). To investigate whether the altered RG-II structure in the hp*GGLT1* silenced lines had affected other pectic domains, the oxalate cell wall fraction was used to perform immune dotblots with a panel of antibodies raided against different pectin epitopes (Figure S5). However, no difference was observed between the EV control and the silenced lines. In combination with the monosaccharide composition data (Figure 2D, Data S1) and the xyloglucan data (Figure S2) we conclude that the reduction in GGLT1 expression does not affect non-RG-II polymers.

These data provide strong evidence that silencing of *GGLT1* leads to a reduction in the abundance of L-galactose on side-chain A of RG-II, and provides additional evidence that the absence of this sugar leads to a decrease in the ability of the RG-II monomer to self-assemble into a borate cross-linked dimer. Moreover, this L-galactose-depleted dimer is less stable in the presence of calcium chelators than its wild-type counterpart, a result consistent

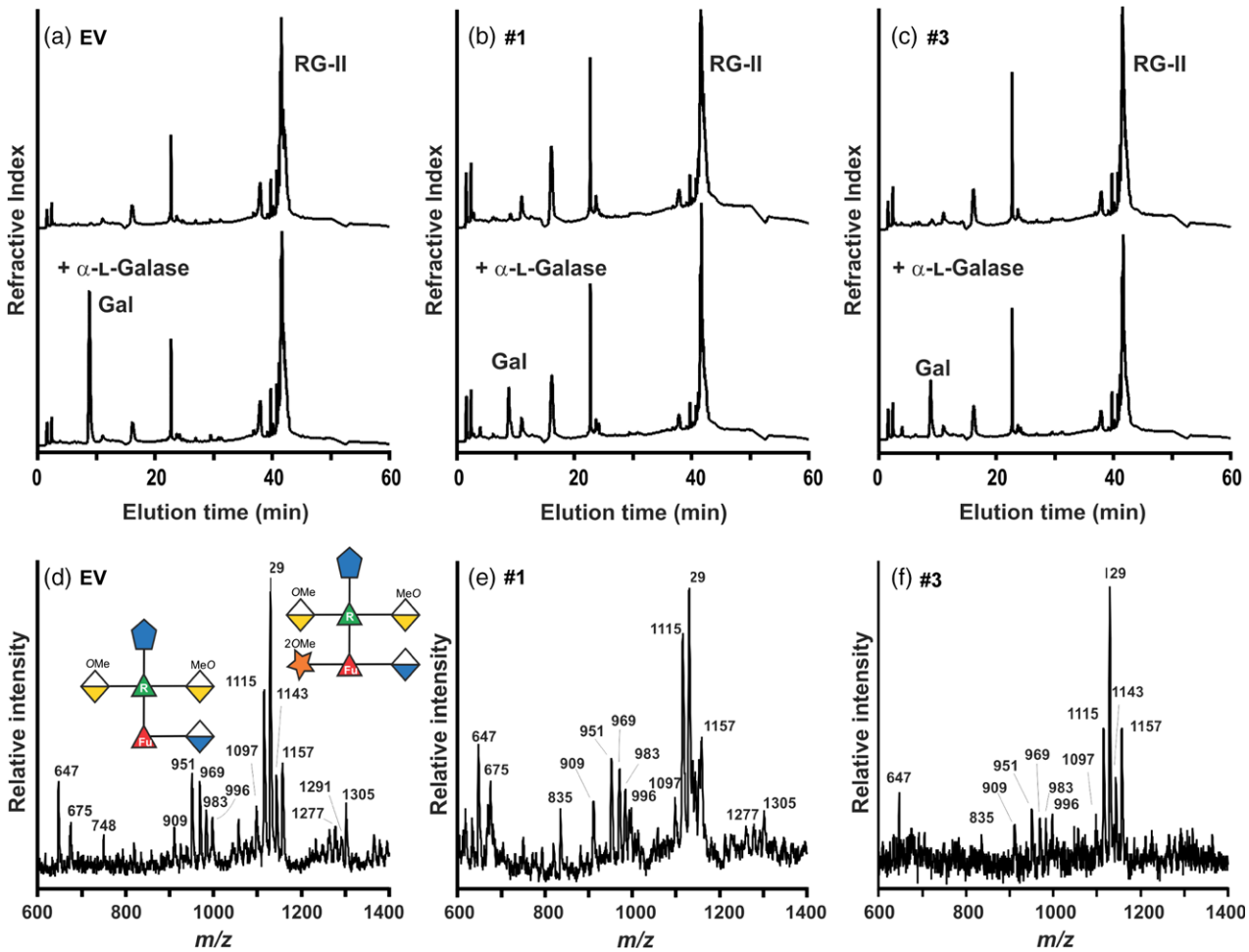

Figure 4. α-L-galactosidase treatment confirms that the rhamnogalacturonan-II (RG-II) from the hairpin (hp) *GGLT1* lines is deficient in α-L-galactose. (a)–(c). The high-performance anion exchange chromatography with pulsed amperometric detection profiles of untreated (top) and α-L-galactosidase-treated (bottom) RG-II from the empty vector (EV) control and hp*GGLT1* lines. The elution position of galactose, which was the only monosaccharide detected, is shown. (d)–(f) The negative ion matrix-assisted laser desorption–ionization time-of-flight mass spectrum of side-chain A generated by selective acid hydrolysis of L-galactosidase-treated RG-II. The predominant oligosaccharide (*m/z* 1115, 1129, 1143 and 1157) corresponds to side-chain A lacking L-galactose. The differences in mass of 14 Da correspond to differences in the extent of *O*-methylation of side-chain A. Only low-intensity signals (*m/z* 1277, 1291 and 1305) corresponding to the L-galactose-containing side-chain A were detected. The oligosaccharide structures are represented using a modified Symbol Nomenclature for Glycans nomenclature. See Figure 1 for details.

with the notion that interactions of borate and calcium with RG-II are important for plant growth (Matoh and Kobayashi, 1998; Feng *et al.*, 2018).

Complementation of hp*GGLT1* growth phenotypes with borate supplementation

Several growth phenotypes, including the dwarf phenotype of *mur1*, that have been attributed to defects in RG-II structure and cross-linking have been reported to be rescued by supplementing the growth medium with additional borate (O'Neill *et al.*, 2001). To further explore the observed growth phenotypes of the hp*GGLT1* lines (Figure 2), plants were grown hydroponically to control the availability of all macro- and micro-nutrients, including borate. In low-borate media the hp*GGLT1* lines are severely stressed, and their rosette diameter is about 70% smaller than that of EV control plants (Figure 5a,b). However, this phenotype is not observed when the silenced plants are grown in high-borate media (Figure 5a,c). The amount of borate in the growth medium did not affect *GGLT1* expression, thereby excluding a potential effect of borate deficiency or supplementation on transgene expression and silencing strength (Figure S6). Therefore, we conclude that partial loss of the RG-II L-galactose decoration in hp*GGLT1* reduces the rate of RG-II borate-dependent dimerization, directly affecting plant development.

Hairpin *GGLT1* plants grown in low-borate conditions have altered cell wall composition and are more easily saccharified

Since hp*GGLT1* plants grown in the presence of 1 mM boric acid or no added boric acid had different phenotypes,

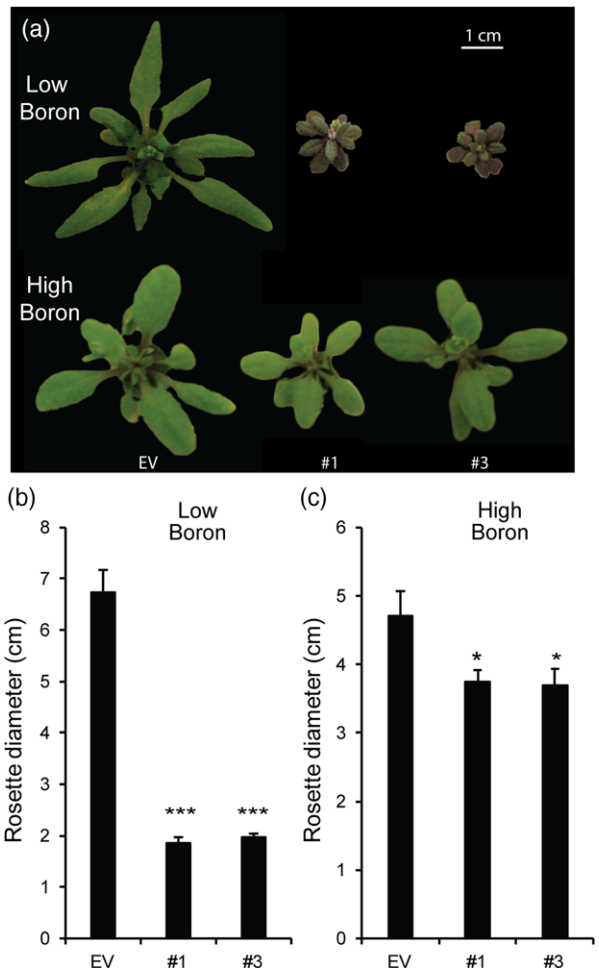

Figure 5. Boron complements hairpin (hp) *GGLT1* phenotypes. Seeds were germinated on agar containing 1/2 MS (which contains 50 μM boric acid) and then grown for 7 days. The seedlings were then transferred to hydroponic growth media containing no added boric acid (low, 0 mM) or 1 mM boric acid (high boron). (a) Representative rosettes of 4-week-old plants. Quantification of rosette diameter in low boron (b) or high boron (c). The data for (b) and (c) represent the mean of 19–25 plants ± SEM. Asterisks indicate a significant difference from the empty vector (EV) (Student's *t*-test, $*P < 0.05$, $**P < 0.01$, $***P < 0.001$). [Colour figure can be viewed at wileyonlinelibrary.com].

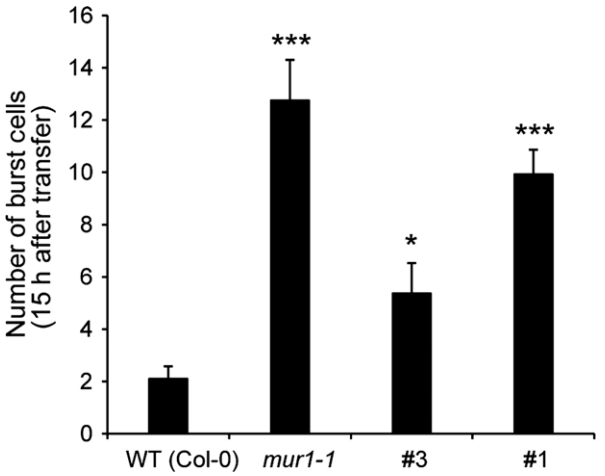

Figure 6. Hairpin (hp) *GGLT1* roots display cell bursting during salt stress. (a) The number of burst cells observed within the first 15 h after salt treatment in the wild type (WT), *mur1* and two *hpGGLT1* lines. (b) Representative time-lapse images of WT, *mur1* and *hpGGLT1* roots after salt treatment. The data for (a) represent the mean of 8–13 plants ± SEM. Asterisks indicate a significant difference from the WT (Student's *t*-test, $*P < 0.05$, $**P < 0.01$, $***P < 0.001$).

we were curious to know if altering the structure and dimerization of RG-II in hp*GGLT1* led to changes in other cell wall components. Therefore we determined the monosaccharide composition of destarched leaf AIR from plants grown under different borate concentrations (Figure S7). No significant visible differences were discernible in hp*GGLT1* and EV plants grown with 1 mM borate (Figure S7D, Data S1). However, we saw increases in the abundance of several neutral monosaccharides, in particular glucose (Figure S7A, Data S1), in the walls of plants grown with no added borate. No differences in aniline blue staining of the walls of EV and hp*GGLT1* lines were observed, suggesting that the increase in non-cellulosic glucose in plants which appear severely stressed (Figure 6a) is not due to callose deposition (Figure S8). Finally, we performed Saeman hydrolysis of the TFA-resistant AIR to determine the amount of glucose derived from crystalline cellulose. A substantial increase in cellulose-derived glucose was detected in the hp*GGLT1* lines grown with no added borate (Figure S4B) but not in plants grown under high-borate conditions (Figure S4E).

To further investigate the altered cell wall in the hp*GGLT1* plants grown with no added borate, we performed a saccharification assay on the destarched AIR to measure the quantity of enzymatically accessible sugars in this material. Following pre-treatment with hot water, the samples were treated with a commercial saccharification cocktail of GHs, and the amount of reducing sugar released after 72 h was measured. As expected, given the increase in cell wall glucose (Figure S4A,B), low-borate-grown hp*GGLT1* plants had a significant increase in the amount of sugar released compared with EV (Figure S4C), a difference that was not seen in high-borate growth conditions (Figure S4F).

Hairpin GGLT1 has impaired cell wall integrity sensing in response to salinity stress

Wall structure is also important for growth under environmental stress (Feng *et al.*, 2018) Salinity stress weakens the wall, probably by disrupting pectin cross-linking (Byrt *et al.*, 2018) . The FERONIA receptor directly binds pectin, and prevents uncontrolled cell expansion caused by salt stress (Feng *et al.*, 2018). Similar to the *fer* mutant, the root cells of *mur1* burst during growth in the presence of salt,

suggesting a role for RG-II cross-linking in allowing roots to recover growth.

Since hp*GGLT1* plants have disrupted RG-II, we predicted that if the FERRONIA model is correct the roots should show a similar loss of wall integrity as *mur1* when grown in the presence of salt. Indeed, compared with the wild type, root cells of hp*GGLT1* plants burst after salt treatment during the growth recovery phase (Figure 6, Movie S1).

The L-ascorbic acid content is increased in leaves of hp*GGLT1* plants

The GDP-L-galactose formed in the cytosol can be converted to L-galactono-1,4-lactone for the synthesis of ascorbic acid (vitamin C) (Dowdle *et al.*, 2007). Thus, a reduction in the activity of a Golgi-localized GDP-L-galactose transporter may lead to increased amounts of cytosolic GDP-L-galactose, thereby increasing the availability of substrate for ascorbic acid formation. Indeed, we found that the hp*GGLT1* lines contain between 59% and 64% more ascorbate than the EV plants (Figure 7).

DISCUSSION

Nucleotide sugar transporters regulate the flow of donor substrates into the Golgi for use by GTs. However, it is challenging to predict the NDP-sugar transported by these enzymes from amino acid sequences alone. Here, we have provided evidence that GGLT is a GDP-L-galactose transporter, and show that it is required for the production of structurally normal RG-II. Reducing *GGLT1* expression led to a decrease in the L-galactose content of RG-II and a reduction in RG-II dimerization and dimer stability. Growth of the silenced plants is rescued by adding additional borate to the growth medium. Thus, suppressing GGLT provides a unique opportunity to investigate the effects of structural changes of RG-II on boron requirements for plant growth.

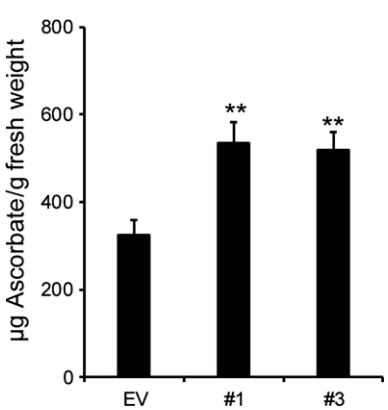

Figure 7. Ascorbic acid content of hp*GGLT1* leaves. Data are the mean of eight to nine plants ± SEM. Asterisks indicate a significant different from EV (Student's *t*-test, $*P < 0.05$, $**P < 0.01$, $***P < 0.001$).

GGLT1 is probably a GDP-L-galactose transporter

Despite multiple reported failures to heterologously express the GGLT1 protein (e.g. Handford *et al.*, 2004), we were able to transiently express GGLT1 as a YFP fusion in onion epidermal cells and confirm its predicted localization to the Golgi apparatus. Unfortunately, as others have also reported, we were unable to express GGLT1 in yeast to perform biochemical analysis of *in vitro* activity. Therefore, we took an *in planta* approach to determine the function of GGLT1. GDP-L-galactose lacked a reported NST, and in wild-type Arabidopsis L-galactose is present only in the pectic polysaccharide RG-II. Analysis of RG-II from hp*GGLT1* plants showed that there was a reduction in RG-II dimer formation, which was correlated with a specific loss of the terminal L-galactose present on side-chain A. We did not detect changes to other biopolymers known to use GDP-mannose, GDP-glucose or GDP-fucose.

Dimerization of RG-II is critical for plant development

We propose that GGLT1, and the L-galactose decoration on RG-II, is essential for plant development and reproduction. This is consistent with previous studies showing that L-galactose is present on side-chain A of all RG-IIs analyzed to date (Voxeur *et al.*, 2011; Pabst *et al.*, 2013; Avci *et al.*, 2018; Wu *et al.*, 2018), with studies suggesting that RG-II is critical for pollen development, pollen germination and seed development, and that plants with abnormal RG-II exhibit major growth defects (Egelund *et al.*, 2006, 2008; Gilbert *et al.*, 2009; Petersen *et al.*, 2009; Fangel *et al.*, 2011; Liu *et al.*, 2011; Voxeur *et al.*, 2011). When the plants were grown in the presence of boric acid, their reduced growth phenotype was partially rescued. This was also reported for GME-silenced tomato plants (Gilbert *et al.*, 2009; Voxeur *et al.*, 2011). While a reduction in GME expression affects the biosynthesis of all GDP-linked sugars, as well as ascorbate, the authors suggested that it was the loss of RG-II dimerization that was critical (Voxeur *et al.*, 2011), and our study supports this conclusion.

It should be noted that the rosette morphology of hp*GGLT1* plants is different from that described for *mur1* or hp*GFT1*, which has been suggested to arise from the replacement of RG-II L-fucose with L-galactose, leading to the incomplete formation of side-chain A (Pabst *et al.*, 2013). Since plants lacking fucose on xyloglucan or arabinogalactan proteins grow normally, the phenotype had been ascribed to reduced RG-II dimerization because of the altered RG-II structure in *mur1* and hp*GFT1*. Our results suggest that either the phenotype is dependent on the exact nature of the RG-II side-chain modification, or that the 'cabbage-like' growth habit of *mur1* and hp*GFT1* results from the loss of fucosylation of another molecule. For example, it has been proposed that fucose is necessary for epidermal growth factor (EGF) domain

activation of receptor-like kinases (Wang *et al.*, 2001), and for promoting the interaction of DELLA with the brassinosteroid pathway (Zentella *et al.*, 2017).

Boron deficiency probably induces stress responses that are impacted when L-galactose transport is disrupted

Boron is an essential micronutrient that is required for normal plant growth and development, and its availability is important for maintaining plant productivity. Too little results in poor plant growth, but too much is toxic. To date, the major described role for boron is to cross-link RG-II (Kobayashi *et al.*, 1996; O'Neill *et al.*, 2004). This has been shown to affect the tensile strength (Ryden *et al.*, 2003) and porosity (Fleischer *et al.*, 1999) of cell walls. In some species, borate deficiency results in cell wall thickening (reviewed in Wang *et al.*, 2015). In our hands, boron-deficient plants did show an increase in cellulose-derived glucose, as well as some hemicellulose derived sugars, including mannose. A cell wall integrity-sensing pathway responsive to salinity stress, and acting via the receptor kinase FER, has recently been described and is thought to act via interaction with pectin (Feng *et al.*, 2018). Here we show that hp*GGLT1* plants display a similar salt-specific loss of cell wall integrity as *fer* and *mur1*. These data suggest that RG-II cross-linking is directly disrupted by salinity, or part of a compensatory feedback loop that is necessary to recover wall strength during acclimation. Such a feedback loop has also been reported in other primary cell wall mutants (Voxeur and Höfte, 2016). Transcriptomic data from plants grown under boron deficiency show altered transcript accumulation for polygalacturonases, pectin methylesterases and pectate lyases, all enzymes involved in cell wall remodeling, as well as stress response genes (Camacho-Cristobal *et al.*, 2008, 2011). The hp*GGLT1* plants will be a useful tool for investigating this process further.

Boron has also been shown to affect the catalytic activities of plasma membrane proteins (enzymes or transporters) (Goldbach and Wimmer, 2007), control the transcription of specific gene targets (e.g. the boron transporter NIP5) (Tanaka *et al.*, 2016) and to affect the homeostasis of oxidative compounds that may alter lipid properties (Shah *et al.*, 2017). More recently, it was proposed that boron may serve as a potential link between RG-II and GIPCs. These are a heavily glycosylated class of sphingolipids and are major components of the plant plasma membrane. Interestingly, this proposed linkage would provide a physical interaction between the plasma membrane and the cell wall (Voxeur and Fry, 2014), and is promising avenue for future investigation.

CONCLUSION

Here we have shown that GGLT1 is a Golgi-localized transporter that probably provides GDP-L-galactose for biosynthesis of RG-II. The hp*GGLT1* knockdown lines have strong developmental defects that are correlated with reduced RG-II dimerization and stability. hp*GGLT1* is the first plant with an altered cell wall in which one specific sugar, L-galactose, is altered only in RG-II. Demonstrating the importance of this glycosyl residue for proper formation and stability of RG-II dimers provides insight into why the structure of RG-II is conserved. Thus, we conclude that GGLT1, L-galactose and structurally complete RG-II are essential for plant growth and development, possibly through cell wall integrity sensing. We believe that the hp*GGLT1*-silenced plants provide new tools for further investigation of the relationship between the structure of RG-II and the response of plants to boron deficiency or overexposure.

EXPERIMENTAL PROCEDURES

Plant growth conditions

Arabidopsis seeds were surface sterilized and sown on solid medium containing 0.5× Murashige and Skoog (MS) salts and sucrose (1% w/v) (Murashige and Skoog, 1962). Following stratification (48–72 h, 4°C, in the dark), plates were transferred to a growth room (22°C, 100–200 μmol m^{-2} sec^{-1}, 14 h light/10 h dark, 60% humidity). After 7 days, plants were transferred to soil or grown hydroponically as described below. All experiments were performed on at least three independently grown biological replicates unless otherwise stated. After transfer to soil, plants were grown in chambers at 22°C, 100–200 μmol m^{-2} sec^{-1}, 60% humidity and cultivated under long-day (16-h light/8-h dark) or short-day (10-h light/14-h dark) conditions.

For hydroponic growth, seedlings were transferred to a plug of rockwool substrate and supported in a microfuge tube (with the end removed) in a modified pipette tip box. The tip box was filled with growth medium (for composition see Simmons *et al.*, 2016). The boron concentration was adjusted as described in the figure legends by the addition of boric acid. After 1 week, the plants were transferred to a larger hydroponics system (5 L volume) equipped with an aquarium pump. Plants were harvested 2 weeks after transfer.

Subcellular localization

GGLT1 was PCR amplified (see Table S2 for the primer sequences used in this study) and inserted into the Gateway™ pDONR™/Zeo vector. The N-terminal YFP fusion was created using the LR Clonase II reaction (Life Technologies, https://www.thermofisher.com/uk/en/home/brands/life-technologies.html) following the manufacturer's protocol. GGLT1-YFP, a *cis*-Golgi marker (α-ManI-49-ECFP) was expressed from the pBullet plasmid as previously reported (Lao *et al.*, 2014). Gold particles were coated with plasmid DNA and biolistically transformed into yellow onion epidermal cells as described (Lao *et al.*, 2014). Sixteen to 24 h after particle bombardment, YFP and CFP fluorescence were observed using a Zeiss LSM 710 (Carl Zeiss, http://www.zeiss.com/).

Hairpin RNA production

A hpRNAi construct targeting *GGLT1* expression was obtained using the Gateway®-compatible pHELLSGATE12 plasmid. A 379-bp PCR-amplified *GGLT1* sequence fragment was inserted into pDONR™ 223 using BP clonase. Insertion of this sequence in

pHELLSGATE12 in both sense and antisense orientations is made possible using a single LR clonase reaction. After transformation of wild-type (ecotype Col-0) Arabidopsis, seeds were selected on 0.5× MS medium supplemented with 1% (w/v) sucrose and kanamycin (50 μg ml^{-1}). Surviving seedlings were transferred to soil. Homozygous T_3 lines were used for all assays. All constructs and seeds generated for this project will be made available via JBEI's Inventory of Composable Elements (https://public-registry.jbei.org/).

Release and isolation of RG-II from AIR of empty vector and *hpGGLT1* lines

To remove starch, AIR (250 mg) was suspended in 25 ml of 0.1 M sodium acetate, pH 5.0, containing 0.01% Thimerosal and treated at 55°C overnight with shaking (250 r.p.m.) with a Spirizyme Excel (30 μl; Novozymes, https://www.novozymes.com/en) and Liquozyme SC DS (150 μl; Novozymes). The suspension was then filtered, and the insoluble residue washed with buffer. To solubilize pectin, the de-starched AIRs were resuspended in 25 ml of 0.5% ammonium oxalate, pH 5.0, containing 0.01% Thimerosal, and shaken at 250 r.p.m. overnight at 21°C. The slurries were filtered through 50-μm nylon mesh layered over a Whatman Grade GF/A filter and washed with additional oxalate. Finally, the oxalate-soluble material, which is enriched in pectin, was dialyzed (3500 molecular weight cut off, MWCO) against deionized water for 2–3 days and lyophilized.

To generate RG-II, solutions of the oxalate-soluble material (20–40 mg) in 50 mM ammonium formate, pH 5 (1 ml), were treated for 16 h at room temperature with endo-polygalacturonase (Megazyme M2, 2 units). The digests were filtered (0.2-μm nylon mesh spin filter) and then portions (200 μl per run) were fractionated on a Superdex™ 75 10/300 GL column with refractive index detection (O'Neill *et al.*, 1996). Fractions were collected manually and repeatedly freeze dried to remove ammonium formate.

Side-chains A and B were released by treating RG-II (1–2 mg) for 1 h at 80°C with 0.1 M TFA (Pabst *et al.*, 2013). The acid was removed under a flow of air. The reside was then dissolved in water and the acidic oligosaccharides enriched using a Supelclean ENVI Carb cartridge (Millipore Sigma, https://www.sigmaaldrich.com/) as described (Packer *et al.*, 1998). The oligosaccharides were then analyzed by MALDI-TOF MS in negative ion mode with a Bruker LT Microflex MALDI-TOF mass spectrometer using a Nafion-coated probe and DHB as the matrix (Jacobs and Dahlman, 2001) and in positive ion mode using a stainless steel probe with DHB as the matrix.

Expression and purification of recombinant α-L-galactosidase (BT1010) from *B. thetaiotaomicron*

Recombinant proteins were produced in *Escherichia coli* Tuner™ (DE3) (Millipore Sigma) cells harboring BT1010 cloned into pET28a in frame with an N-terminal His_6 tag, and purified as described (Ndeh *et al.*, 2017) with minor modifications. Briefly, cells were cultured at 37°C in Luria–Bertani (LB) medium supplemented with kanamycin (50 μg ml^{-1}) to mid-exponential phase ($OD_{600\ nm}$ = 0.6-0.8). Recombinant protein expression was induced by the addition of isopropyl-β-D-1-thiogalactopyranoside (IPTG, 0.1 mM) and allowed to proceed overnight at 16°C. Cells were lysed by sonication, and His^6-tagged BT1010 was purified from cell-free extracts by immobilized metal affinity chromatography (IMAC) using HisPur™ Cobalt Resin (ThermoFisher Scientific, https://www.thermofisher.com/). Purified protein was dialyzed against sodium acetate (NaOAc; 50 mM, pH 5.5) using D-Tube™ Dialyzer Maxi devices (MWCO 6–8 kDa; EMD Millipore, http://www.emdmillipore.com/) and used directly for enzymatic hydrolysis.

Treatment of RG-II with the α-L-galactosidase (BT1010) from *B. thetaiotaomicron*

The RG-II isolated from the empty vector and hp*GGLT1* lines (1–2 mg) was converted to the monomer by treatment for 1 h at room temperature with 0.1 M HCl (O'Neill *et al.*, 1996). The solutions were dialyzed (3500 MWCO) against deionized water and freeze dried. Solutions (200 μl) of the monomer in NaOAc (25 mM, pH 5) were then treated for 24 h at room temperature with the recombinant α-L-galactosidase (BT1010, 9 μg protein) from *B. thetaiotaomicron* (Ndeh *et al.*, 2017). Each reaction mixture was desalted using a Dionex OnGuard H cartridge (1 ml, ThermoFisher) and freeze dried. The desalted material was dissolved in water (200 μl) and an aliquot (10–20 μl) analyzed by HPAEC PAD to confirm that galactose had been released by the α-L-galactosidase. An equal volume of 0.2 M TFA was then added to the remaining material and the mixture heated for 1 h at 80°C. The cooled solution was concentrated to dryness under a flow of air. The material was dissolved in water and the acidic oligosaccharides enriched using a Supelclean ENVI Carb cartridge (Sigma Aldrich, http://www.sigmaaldrich.com/) as described (Packer *et al.*, 1998). The oligosaccharides were then analyzed by MALDI-TOF MS in negative-ion mode using a Nafion-coated probe and DHB as the matrix (Jacobs and Dahlman, 2001).

Immuno-dot blots

The oxalate-isolated, pectin-rich fraction described above was resuspended in water at a final concentration of 0.5 mg ml^{-1}. The samples were then serially diluted using water and 1 μl was spotted onto nitrocellulose membrane and allowed to air dry overnight. The membrane was briefly washed with 1× phosphate buffered saline (PBS), and then incubated with 5% (w/v) non-fat dairy milk (NFDM) dissolved in 1× PBS for 1 h at room temperature, with gentle agitation. The membrane was then incubated overnight (4°C, gentle agitation) in 5% (w/v) NFDM in 1× PBS containing the primary antibody (1:300 dilution). Following three 5-min washes in 1× PBS, the membrane was then incubated for 1 h at room temperature (gentle agitation) in 5% (w/v) NFDM in 1× PBS containing the secondary antibody (horseradish peroxidase-linked anti-rat antibody at 1:5000 dilution). The membrane was then washed in 1× PBS (four 5-min washes). The blots were developed with an enhanced chemiluminescence (ECL) detection reagent (Bio-Rad, http://www.bio-rad.com/) according to the manufacturer's instructions and visualized using an Imager 600 (GE Healthcare Life Sciences, https://www.gelifesciences.com). The primary antibodies were obtained from either Professor Paul Knox, University of Leeds (http://www.plantprobes.net/; LM5, LM6, LM19 and LM20) or Professor Michael Hahn, CCRC, University of Georgia (https://www.ccrc.uga.edu/~carbosource/CSS_home.html; CCRC-M35) (Jones *et al.*, 1997; Willats *et al.*, 1998; Verhertbruggen *et al.*, 2009; Pattathil *et al.*, 2010). Experiements with negative controls (water) and positive controls (commercial preparations of the polysaccharides) were performed alongside.

Cell wall monosaccharide composition

Plant tissue (age and type as specified in the figure legends) was harvested, submerged in 96% (v/v) ethanol and boiled at 70°C for 30 min. Following homogenization using a ball mill (Retsch,

https://www.retsch.com/), the pellet was collected by centrifugation (4000 × ***g*** for 15 min). The pellet was then washed with 100% (v/v) ethanol and twice with chloroform:methanol (2:1), followed by successive washes with 65% (v/v), 80% (v/v) and 100% (v/v) ethanol. The remaining pellet of AIR was dried at 40°C overnight. To remove starch, the AIR was treated exhaustively with a cocktail of α-amylase, amyloglucosidase and pullulanase as described (Harholt *et al.*, 2006).

The monosaccharide composition of the non-cellulosic fraction was determined by hydrolysis of 100 μg AIR with 2 M TFA for 1 h at 120°C. After cooling and centrifugation, the supernatant was dried under a vacuum, resuspended in 200 μl of water and retained for analysis. To obtain the glucose content of the crystalline cellulose fraction, the TFA-insoluble pellet was washed with water and further hydrolyzed with 72% (v/v) sulfuric acid for 1 h at room temperature. The sulfuric acid was then diluted to 1 M with water and the samples incubated at 100°C for 3 h and neutralized with $BaCO_3$. All samples were filtered using a 22-μm syringe filter, and quantified by HPAEC-PAD on a Dionex ICS-5000 instrument (ThermoFisher Scientific) as described (Fang *et al.*, 2016).

Saccharification assay

Leaf AIR (2 mg) from hydroponically grown plants, prepared as described above, was mixed with 136 μl of water, agitated at 1400 r.p.m. (30°C, 30 min), and autoclaved at 120°C for 1 h. Saccharification was initiated by adding 260 μl of 100 mM sodium citrate buffer pH 5.0 containing 80 μg ml^{-1} tetracycline and 0.5% (w/w) Cellic CTec2 cellulase (Novozymes). After incubation for 72 h at 50°C with shaking (800 r.p.m.), samples were centrifuged (20 000 × ***g***, 3 min) and 10 μl of the supernatant was collected for measurement of reducing sugars using the 3,5-dinitrosalicylic acid assay and glucose as a standard (Miller, 1959).

Ascorbic acid measurement

The ascorbate content of leaves was measured according to Gautier *et al.* (2009) with modifications. Frozen tissue (1 g) was homogenized, resuspended in 600 μl of 6% (v/v) trichloroacetic acid (TCA) and vortexed until thawed. Following incubation on ice for 15 min, the samples were centrifuged (16 000 × ***g***, 4°C, 15 min). The supernatants (20 μl) were placed in individual wells of a microtiter plate containing 20 μl of 5 mM DTT (in 0.4 M PO_4 buffer, pH 7.4), and kept for 20 min at 37°C, before adding 10 μl of 0.5% (w/v) *N*-ethylmaleimide. After 1 min at 21°C, 80 μl of color reagent was added [solution A, 31% (w/v) orthophosphoric acid, 4.6% (v/v) TCA and 0.6% (w/v) $FeCl_2$; solution B, 4% (w/v) 2,2-dipyridyl in 70% (v/v) ethanol; A:B, 2.75:1] and plates were incubated at 37°C for 40 min. Ascorbic acid standards (0–50 nmol) were included to allow quantification. The plate was scanned at 550 nm using a Spectramax M2 plate reader (Molecular Devices, https://www.moleculardevices.com/).

Aniline blue

Rosette leaves were collected and fixed in acetic acid:ethanol 95% (3:1) for 1 h at room temperature. Fixed leaves were then treated with 2 M NaOH for 2 h prior to neutralization in 50 mM $NaPO_4$ buffer (pH 6.8) for 10 min, and immersion in aniline blue solution (0.01% w/v in 50 mM $NaPO_4$ pH 6.8) was done overnight. Images were obtained with an epifluorescence microscope (Leica MZ 16F, https://www.leica-microsystems.com/).

Extraction and analysis of GIPCs

The sphingolipids content was quantified by LC-MS/MS as described previously (Fang *et al.*, 2016), with modifications. Lyophilized leaves (10 mg) were homogenized and incubated in 800 μl of methanol/1-butanol/1 N KOH (2:3:3) at 50°C for 30 min. The homogenate was acidified by the addition of 450 μl of 1 N HCl, and 1 ml of water and 1-butanol was added for phase separation. The organic layer was dried, dissolved in tetrahydrofuran/methanol/water (2:1:2, v/v/v) containing 0.1% formic acid and analyzed by LC-MS/MS. Lipid content was calculated using internal standards (Fang *et al.*, 2016).

For TLC analysis, lyophilized leaves were homogenized and then incubated at 50°C for 15 min in the lower layer of a isopropanol: hexane:water 55:20:25 solution. The supernatant was retained, and the extraction was repeated on the pellet. The combined supernatants were dried under N_2 and resuspended in methylamine (33% v/v) in ethanol:water (7:3), and incubated at 50°C for 1 h. The supernatant was dried under N_2 and resuspended in chloroform: ethanol:ammonia:water (10:60:6:24), and incubated overnight at room temperature. Following anion exchange (Strata X-AW 33 μm, Phenomenex, http://www.phenomenex.com/) as previously described (Fang *et al.*, 2016), the enriched GIPCs were spotted onto TLC plates and developed in chloroform/methanol/(4 M ammonium hydroxide + 1.8 M ammonium acetate) (9:7:2) buffer. The plate was stained first with primuline [10 mg/100 ml of acetone/water 8:2 (v/v)], a solution that binds to lipids, and observed under 460-nm light. The plate was then stained with orcinol (5% v/v sulfuric acid in ethanol) to detect sugars.

Quantitative PCR

RNA was extracted from the leaves of 1-month old plants grown in long-day conditions in soil or in hydroponics (as specified in the figure legends), using the RNeasy RNA Plant kit (Qiagen, http://www.qiagen.com/). A total of 0.5–1 μg RNA was reverse-transcribed into cDNA with Superscript II reverse transcriptase (ThermoFisher Scientific) and $d(T)_{20}$ oligomers (IDT). To determine *GGLT1* and *GFT1* expression, the resultant cDNA was subsequently used as the template in a qPCR reaction containing 2× QuantiFast SYBR Green PCR Kit Master Mix (Qiagen) (plants grown in soil) or 2× SYBR Select Master Mix (Applied Biosystems, https://www.thermofisher.com) (plants grown hydroponically) and gene-specific primers for *GGLT1* and *GFT1.* Expression of Arabidopsis *PP2A* (*At1g13320*) and a SAND family gene (*At2g28390*) was quantified (see Table S2 for all primer sequences), as these have previously been established as housekeeping genes (Czechowski *et al.*, 2005). The PCR reactions were performed using the CFX96 Touch System real-time PCR detection system (Bio-Rad) and the following thermal profile was used for all PCR reactions: 95°C for 5 min, 40 cycles of 95°C for 10 sec and 60°C for 30 sec.

Cell Integrity assays

Live imaging of roots was performed as previously described (Feng *et al.*, 2018). Five-day-old seedlings cultured on 1× MS, 1% (w/v) sucrose pH 5.7 Gelrite media were transferred to media supplemented with 140 mM NaCl in a moisture chamber made from a 60 × 15-mm Petri dish (Fisher Scientific, AS4052). Bright-field images of the root tip area were captured every 15 min from a Leica DMI6000 inverted compound microscope with HC PL APO 10×/0.4 CS objective (Leica) and LAS software (Leica). Images were then stitched together using the ImageJ 'Pairwise

Stitching' plugin. Cell bursting events were manually quantified from the resulting movies. Events in which root cells rapidly lost volume or appeared opaque were quantified as a cell-bursting event.

ACKNOWLEDGEMENTS

The authors wish to thank Paul Dupree for helpful discussions.

CONFLICTS OF INTEREST

The authors declare no conflicts of interest.

FUNDING INFORMATION

This work was funded as part of the DOE Joint BioEnergy Institute (http://www.jbei.org) supported by the US Department of Energy, Office of Science, Office of Biological and Environmental Research, through contract DE-AC02-05CH11231 between Lawrence Berkeley National Laboratory and the US Department of Energy (JS, SH, MC, KSK, JCM). MAO, BRU and AA were supported by a grant from The Division of Chemical Sciences, Geosciences, and Biosciences, Office of Basic Energy Sciences of the US Department of Energy. We also acknowledge the U.S. Department of Energy-funded Center for Plant and Microbial Complex Carbohydrates (grant DE-FG02-96ER20220) for equipment support. This work was also supported partially by JSPS KAKENHI 17K15411 to TI and 26292190 to MK-Y. Funding was provided by grants from the National Science Foundation (NSF) Plant Genome Research Program (IOS 1238202), NIH NIGMS (R01 GM123259-01) and Carnegie Institution for Science Endowment to JRD.

SUPPORTING INFORMATION

Additional Supporting Information may be found in the online version of this article.

Figure S1. Subcellular localization of GGLT1.

Figure S2. Xyloglucan composition is unaffected in hp*GGLT1.*

Figure S3. Thin-layer chromatography analysis of an enriched glycosylinositolphosphorylceramide fraction from the empty vector and hairpin *GGLT1.*

Figure S4. Matrix-assisted laser desorption–ionization analysis of rhamnogalacturonan-II side-chain B.

Figure S5. Immuno-dot blot of oxalate fraction shows unchanged bulk pectin.

Figure S6. GGLT1 silencing is not dependent on boron availability.

Figure S7. Cell wall composition is altered when hairpin *GGLT1* is grown in boron-deficient conditions.

Figure S8. Callose deposition in empty vector and hairpin *GGLT1* leaves.

Table S1. The abundance of the rhamnogalacturonan-II dimer and monomer in the material released by endopolygalacturonase (EPG) treatment of the alcohol-insoluble residue and by EPG treatment of the ammonium oxalate soluble pectin.

Table S2. Sequences of the oligonucleotide primers used in this paper.

Data S1. Data underlying graphs included in this paper, including complete monosaccharide composition data.

Data S2. Sphingolipidomic data.

Movie S1. Root cell bursting in response to salinity in (top-bottom) the wild type, *mur1-1*, *hpGGLT1*-#3 and *hpGGLT1*-#1.

REFERENCES

Ahn, J.W., Verma, R., Kim, M., Lee, J.Y., Kim, Y.K., Bang, J.W., Reiter, W.D. and Pai, H.S. (2006) Depletion of UDP-D-apiose/UDP-D-xylose synthases results in rhamnogalacturonan-II deficiency, cell wall thickening, and cell death in higher plants. *J. Biol. Chem.* **281**, 13708–13716.

Atmodjo, M.A., Hao, Z. and Mohnen, D. (2013) Evolving views of pectin biosynthesis. *Annu. Rev. Plant Biol.* **64**, 747–779.

Avci, U., Pena, M.J. and O'Neill, M.A. (2018) Changes in the abundance of cell wall apiogalacturonan and xylogalacturonan and conservation of rhamnogalacturonan II structure during the diversification of the Lemnoideae. *Planta*, **247**, 953–971.

Baldwin, T.C., Handford, M.G., Yuseff, M.I., Orellana, A. and Dupree, P. (2001) Identification and characterization of GONST1, a Golgi-localized GDP-mannose transporter in Arabidopsis. *Plant Cell*, **13**, 2283–2295.

Bar-Peled, M. and O'Neill, M.A. (2011) Plant nucleotide sugar formation, interconversion, and salvage by sugar recycling. *Annu. Rev. Plant Biol.* **62**, 127–155.

Baydoun, E.A.H. and Fry, S.C. (1988) [2-3H]mannose incorporation in cultured plant cells: investigation of L-galactose residues of the primary cell wall. *J. Plant Physiol.* **132**, 484–490.

Bonin, C.P., Potter, I., Vanzin, G.F. and Reiter, W.D. (1997) The *MUR1* gene of *Arabidopsis thaliana* encodes an isoform of GDP-D-mannose-4,6-dehydratase, catalyzing the first step in the de novo synthesis of GDP-L-fucose. *Proc. Natl Acad. Sci. USA* **94**, 2085–2090.

Byrt, C.S., Munns, R., Burton, R.A., Gilliham, M. and Wege, S. (2018) Root cell wall solutions for crop plants in saline soils. *Plant Sci.* **69**, 47–55.

Camacho-Cristobal, J.J., Rexach, J. and Gonzalez-Fontes, A. (2008) Boron in plants: deficiency and toxicity. *J. Integr. Plant Biol.* **50**, 1247–1255.

Camacho-Cristobal, J.J., Rexach, J., Herrera-Rodriguez, M.B., Navarro-Gochicoa, M.T. and Gonzalez-Fontes, A. (2011) Boron deficiency and transcript level changes. *Plant Sci.* **181**, 85–89.

Chormova, D., Messenger, D.J. and Fry, S.C. (2014) Boron bridging of rhamnogalacturonan-II, monitored by gel electrophoresis, occurs during polysaccharide synthesis and secretion but not post-secretion. *Plant J.* **77**, 534–546.

Czechowski, T., Stitt, M., Altmann, T., Udvardi, M.K. and Scheible, W.-R. (2005) Genome-wide identification and testing of superior reference genes for transcript normalization in Arabidopsis. *Plant Physiol.* **139**, 5–17.

Davis, J., Brandizzi, F., Liepman, A.H. and Keegstra, K. (2010) Arabidopsis mannan synthase CSLA9 and glucan synthase CSLC4 have opposite orientations in the Golgi membrane. *Plant J.* **64**, 1028–1037.

Delmas, F., Petit, J., Joubes, J., Seveno, M., Paccalet, T., Hernould, M., Lerouge, P., Mouras, A. and Chevalier, C. (2003) The gene expression and enzyme activity of plant 3-deoxy-D-manno-2-octulosonic acid-8-phosphate synthase are preferentially associated with cell division in a cell cycle-dependent manner. *Plant Physiol.* **133**, 348–360.

Delmas, F., Seveno, M., Northey, J.G., Hernould, M., Lerouge, P., McCourt, P. and Chevalier, C. (2008) The synthesis of the rhamnogalacturonan II component 3-deoxy-D-manno-2-octulosonic acid (Kdo) is required for pollen tube growth and elongation. *J. Exp. Bot.* **59**, 2639–2647.

Dowdle, J., Ishikawa, T., Gatzek, S., Rolinski, S. and Smirnoff, N. (2007) Two genes in Arabidopsis thaliana encoding GDP-L-galactose phosphorylase are required for ascorbate biosynthesis and seedling viability. *Plant J.* **52**, 673–689.

Egelund, J., Petersen, B.L., Motawia, M.S., Damager, I., Faik, A., Olsen, C.E., Ishii, T., Clausen, H., Ulvskov, P. and Geshi, N. (2006) Arabidopsis thaliana RGXT1 and RGXT2 encode Golgi-localized (1,3)-alpha-D-xylosyltransferases involved in the synthesis of pectic rhamnogalacturonan-II. *Plant Cell*, **18**, 2593–2607.

Egelund, J., Damager, I., Faber, K., Olsen, C.E., Ulvskov, P. and Petersen, B.L. (2008) Functional characterisation of a putative rhamnogalacturonan II specific xylosyltransferase. *FEBS Lett.* **582**, 3217–3222.

Fang, L., Ishikawa, T., Rennie, E.A. *et al.* (2016) Loss of inositol phosphorylceramide sphingolipid mannosylation induces plant immune responses and reduces cellulose content in Arabidopsis. *Plant Cell*, **28**, 2991–3004.

Fangel, J.U., Petersen, B.L., Jensen, N.B., Willats, W.G., Bacic, A. and Egelund, J. (2011) A putative *Arabidopsis thaliana* glycosyltransferase, At4g01220,

which is closely related to three plant cell wall-specific xylosyltransferases, is differentially expressed spatially and temporally. *Plant Sci.* **180**, 470–479.

Feng, W., Kita, D., Peaucelle, A. *et al.* (2018) The FERONIA receptor kinase maintains cell-wall integrity during salt stress through Ca^{2+} signaling. *Curr. Biol.* **28**(666–675), e665.

Fleischer, A., O'Neill, M.A. and Ehwald, R. (1999) The pore size of non-graminaceous plant cell walls is rapidly decreased by borate ester cross-linking of the pectic polysaccharide rhamnogalacturonan II. *Plant Physiol.* **121**, 829–838.

Funakawa, H. and Miwa, K. (2015) Synthesis of borate cross-linked rhamnogalacturonan II. *Front. Plant Sci.* **6**, 223.

Gautier, H., Massot, C., Stevens, R., Serino, S. and Genard, M. (2009) Regulation of tomato fruit ascorbate content is more highly dependent on fruit irradiance than leaf irradiance. *Ann. Bot.* **103**, 495–504.

Gilbert, L., Alhagdow, M., Nunes-Nesi, A. *et al.* (2009) GDP-D-mannose 3,5-epimerase (GME) plays a key role at the intersection of ascorbate and non-cellulosic cell-wall biosynthesis in tomato. *Plant J.* **60**, 499–508.

Goldbach, H.E. and Wimmer, M.A. (2007) Boron in plants and animals: is there a role beyond cell-wall structure? *J. Plant Nutr. Soil Sci.* **170**, 39–48.

Handford, M.G., Sicilia, F., Brandizzi, F., Chung, J.H. and Dupree, P. (2004) *Arabidopsis thaliana* expresses multiple Golgi-localised nucleotide-sugar transporters related to GONST1. *Mol. Genet. Genomics*, **272**, 397–410.

Hantus, S., Pauly, M., Darvill, A.G., Albersheim, P. and York, W.S. (1997) Structural characterization of novel L-galactose-containing oligosaccharide subunits of jojoba seed xyloglucans. *Carbohyd. Res.* **304**, 11–20.

Harholt, J., Jensen, J.K., Sorensen, S.O., Orfila, C., Pauly, M. and Scheller, H.V. (2006) ARABINAN DEFICIENT 1 is a putative arabinosyltransferase involved in biosynthesis of pectic arabinan in Arabidopsis. *Plant Physiol.* **140**, 49–58.

Jacobs, A. and Dahlman, O. (2001) Enhancement of the quality of MALDI mass spectra of highly acidic oligosaccharides by using a nafion-coated probe. *Anal. Chem.* **73**, 405–410.

Jones, L., Seymour, G.B. and Knox, J.P. (1997) Localization of pectic galactan in tomato cell walls using a monoclonal antibody specific to (1[->]4)-[beta]-D-galactan. *Plant Physiol.* **113**, 1405–1412.

Kobayashi, M., Matoh, T. and Azuma, J. (1996) Two chains of rhamnogalacturonan II are cross-linked by borate-diol ester bonds in higher plant cell walls. *Plant Physiol.* **110**, 1017–1020.

Lao, J., Oikawa, A., Bromley, J.R. *et al.* (2014) The plant glycosyltransferase clone collection for functional genomics. *Plant J.* **79**, 517–529.

Lerouxel, O., Choo, T.S., Seveno, M., Usadel, B., Faye, L., Lerouge, P. and Pauly, M. (2002) Rapid structural phenotyping of plant cell wall mutants by enzymatic oligosaccharide fingerprinting. *Plant Physiol.* **130**, 1754–1763.

Liu, X.-L., Liu, L., Niu, Q.-K., Xia, C., Yang, K.-Z., Li, R., Chen, L.-Q., Zhang, X.-Q., Zhou, Y. and Ye, D. (2011) MALE GAMETOPHYTE DEFECTIVE 4 encodes a rhamnogalacturonan II xylosyltransferase and is important for growth of pollen tubes and roots in Arabidopsis. *Plant J.* **65**, 647–660.

Lombard, V., Golaconda Ramulu, H., Drula, E., Coutinho, P.M. and Henrissat, B. (2014) The carbohydrate-active enzymes database (CAZy) in 2013. *Nucleic Acids Res.* **42**, D490–D495.

Matoh, T. and Kobayashi, M. (1998) Boron and calcium, essential inorganic constituents of pectic polysaccharides in higher plant cell walls. *J. Plant. Res.* **111**, 179–190.

Matsunaga, T., Ishii, T., Matsumoto, S., Higuchi, M., Darvill, A., Albersheim, P. and O'Neill, M.A. (2004) Occurrence of the primary cell wall polysaccharide rhamnogalacturonan II in pteridophytes, lycophytes, and bryophytes. Implications for the evolution of vascular plants. *Plant Physiol.* **134**, 339–351.

Miller, G.L. (1959) Use of dinitrosalicylic acid reagent for determination of reducing sugar. *Anal. Chem.* **31**, 426–428.

Mølhøj, M., Verma, R. and Reiter, W.-D. (2003) The biosynthesis of the branched-chain sugar d-apiose in plants: functional cloning and characterization of a UDP-d-apiose/UDP-d-xylose synthase from Arabidopsis. *Plant J.* **35**, 693–703.

Mortimer, J.C., Yu, X., Albrecht, S. *et al.* (2013) Abnormal glycosphingolipid mannosylation triggers salicylic acid-mediated responses in Arabidopsis. *Plant Cell*, **25**, 1881–1894.

Mounet-Gilbert, L., Dumont, M., Ferrand, C. *et al.* (2016) Two tomato GDP-D-mannose epimerase isoforms involved in ascorbate biosynthesis play specific roles in cell wall biosynthesis and development. *J. Exp. Bot.* **67**, 4767–4777.

Murashige, T. and Skoog, F. (1962) A revised medium for rapid growth and bio assays with tobacco tissue cultures. *Physiol. Plant.* **15**, 473–497.

Ndeh, D., Rogowski, A., Cartmell, A. *et al.* (2017) Complex pectin metabolism by gut bacteria reveals novel catalytic functions. *Nature*, **544**, 65–70.

O'Neill, M.A., Warrenfeltz, D., Kates, K., Pellerin, P., Doco, T., Darvill, A.G. and Albersheim, P. (1996) Rhamnogalacturonan-II, a pectic polysaccharide in the walls of growing plant cell, forms a dimer that is covalently cross-linked by a borate ester. In vitro conditions for the formation and hydrolysis of the dimer. *J. Biol. Chem.* **271**, 22923–22930.

O'Neill, M.A., Eberhard, S., Albersheim, P. and Darvill, A.G. (2001) Requirement of borate cross-linking of cell wall rhamnogalacturonan II for Arabidopsis growth. *Science*, **294**, 846–849.

O'Neill, M.A., Ishii, T., Albersheim, P. and Darvill, A.G. (2004) Rhamnogalacturonan II: structure and function of a borate cross-linked cell wall pectic polysaccharide. *Annu. Rev. Plant Biol.* **55**, 109–139.

Pabst, M., Fischl, R.M., Brecker, L., Morelle, W., Fauland, A., Kofeler, H., Altmann, F. and Leonard, R. (2013) Rhamnogalacturonan II structure shows variation in the side chains monosaccharide composition and methylation status within and across different plant species. *Plant J.* **76**, 61–72.

Packer, N.H., Lawson, M.A., Jardine, D.R. and Redmond, J.W. (1998) A general approach to desalting oligosaccharides released from glycoproteins. *Glycoconj. J.* **15**, 737–747.

Pattathil, S., Avci, U., Baldwin, D. *et al.* (2010) A comprehensive toolkit of plant cell wall glycan-directed monoclonal antibodies. *Plant Physiol.* **153**, 514–525.

Petersen, B.L., Egelund, J., Damager, I., Faber, K., Krüger Jensen, J., Yang, Z., Bennett, E.P., Scheller, H.V. and Ulvskov, P. (2009) Assay and heterologous expression in *Pichia pastoris* of plant cell wall type-II membrane anchored glycosyltransferases. *Glycoconj. J.* **26**, 1235.

Popper, Z.A. and Fry, S.C. (2008) Xyloglucan-pectin linkages are formed intra-protoplasmically, contribute to wall-assembly, and remain stable in the cell wall. *Planta*, **227**, 781–794.

Rautengarten, C., Ebert, B., Moreno, I. *et al.* (2014) The Golgi localized bifunctional UDP-rhamnose/UDP-galactose transporter family of Arabidopsis. *Proc. Natl Acad. Sci. USA* **111**, 11563–11568.

Rautengarten, C., Ebert, B., Liu, L., Stonebloom, S., Smith-Moritz, A.M., Pauly, M., Orellana, A., Scheller, H.V. and Heazlewood, J.L. (2016) The Arabidopsis Golgi-localized GDP-L-fucose transporter is required for plant development. *Nat. Commun.* **7**, 12119.

Reiter, W.D., Chapple, C.C. and Somerville, C.R. (1993) Altered growth and cell walls in a fucose-deficient mutant of Arabidopsis. *Science*, **261**, 1032–1035.

Rogowski, A., Briggs, J.A., Mortimer, J.C. *et al.* (2015) Glycan complexity dictates microbial resource allocation in the large intestine. *Nat. Commun.* **6**, 7481.

Ryden, P., Sugimoto-Shirasu, K., Smith, A.C., Findlay, K., Reiter, W.D. and McCann, M.C. (2003) Tensile properties of Arabidopsis cell walls depend on both a xyloglucan cross-linked microfibrillar network and rhamnogalacturonan II-borate complexes. *Plant Physiol.* **132**, 1033–1040.

Shah, A., Wu, X., Ullah, A., Fahad, S., Muhammad, R., Yan, L. and Jiang, C. (2017) Deficiency and toxicity of boron: alterations in growth, oxidative damage and uptake by citrange orange plants. *Ecotoxicol. Environ. Saf.* **145**, 575–582.

Simmons, T.J., Mortimer, J.C., Bernardinelli, O.D., Poppler, A.C., Brown, S.P., deAzevedo, E.R., Dupree, R. and Dupree, P. (2016) Folding of xylan onto cellulose fibrils in plant cell walls revealed by solid-state NMR. *Nat. Commun.* **7**, 13902.

Smirnoff, N. (2000) Ascorbate biosynthesis and function in photoprotection. *Phil. Trans. R. Soc. B: Biol. Sci.* **355**, 1455–1464.

Tan, L., Eberhard, S., Pattathil, S. *et al.* (2013) An Arabidopsis cell wall proteoglycan consists of pectin and arabinoxylan covalently linked to an arabinogalactan protein. *Plant Cell*, **25**, 270–287.

Tanaka, M., Sotta, N., Yamazumi, Y. *et al.* (2016) The minimum open reading frame, AUG-stop, induces boron-dependent ribosome stalling and mRNA degradation. *Plant Cell*, **28**(11), 2830–2849.

Varki, A., Cummings, R.D., Aebi, M. *et al.* (2015) Symbol nomenclature for graphical representations of glycans. *Glycobiology*, **25**, 1323–1324.

Verhertbruggen, Y., Marcus, S.E., Haeger, A., Ordaz-Ortiz, J.J. and Knox, J.P. (2009) An extended set of monoclonal antibodies to pectic homogalacturonan. *Carbohyd. Res.* **344**, 1858–1862.

Voxeur, A. and Fry, S.C. (2014) Glycosylinositol phosphorylceramides from Rosa cell cultures are boron-bridged in the plasma membrane and form complexes with rhamnogalacturonan II. *Plant J.* **79**, 139–149.

Voxeur, A. and Höfte, H. (2016) Cell wall integrity signaling in plants: "To grow or not to grow that's the question". *Glycobiology*, **26**, 950–960.

Voxeur, A., Gilbert, L., Rihouey, C., Driouich, A., Rothan, C., Baldet, P. and Lerouge, P. (2011) Silencing of the GDP-D-mannose 3,5-epimerase affects the structure and cross-linking of the pectic polysaccharide rhamnogalacturonan II and plant growth in tomato. *J. Biol. Chem.* **286**, 8014–8020.

Wang, Y., Shao, L., Shi, S., Harris, R.J., Spellman, M.W., Stanley, P. and Haltiwanger, R.S. (2001) Modification of epidermal growth factor-like repeats with O-fucose. Molecular cloning and expression of a novel GDP-fucose protein O-fucosyltransferase. *J. Biol. Chem.* **276**, 40338–40345.

Wang, N., Yang, C., Pan, Z., Liu, Y. and Peng, S.A. (2015) Boron deficiency in woody plants: various responses and tolerance mechanisms. *Front. Plant Sci.* **6**, 916.

Willats, W.G., Marcus, S.E. and Knox, J.P. (1998) Generation of monoclonal antibody specific to (1–>5)-alpha-L-arabinan. *Carbohyd. Res.* **308**, 149–152.

Wu, D., Cui, L., Yang, G., Ning, X., Sun, L. and Zhou, Y. (2018) Preparing rhamnogalacturonan II domains from seven plant pectins using Penicillium oxalicum degradation and their structural comparison. *Carbohydr. Polym.* **180**, 209–215.

Zentella, R., Sui, N., Barnhill, B. *et al.* (2017) The Arabidopsis O-fucosyltransferase SPINDLY activates nuclear growth repressor DELLA. *Nat. Chem. Biol.* **13**, 479–485.